Journal of Controlled Release 372 (2024) 522–530

Contents lists available at ScienceDirect

Journal of Controlled Release

journal homepage: www.elsevier.com/locate/jconrel

Tuning the photophysical properties of cyanine by barbiturate functionalization and nanoformulation for efficient optoacoustics-guided phototherapy

Nian Liu [a,b,c], Patrick O'Connor [d,e], Vipul Gujrati [b,c,*], Divyesh Shelar [c], Xiaopeng Ma [f], Pia Anzenhofer [c], Uwe Klemm [c], Xinhui Su [a], Yuanhui Huang [b], Karin Kleigrewe [g], Annette Feuchtinger [h], Axel Walch [h], Michael Sattler [e,i], Oliver Plettenburg [d,j], Vasilis Ntziachristos [b,c,*]

[a] Department of Nuclear Medicine, The First Affiliated Hospital, Zhejiang University School of Medicine, Hangzhou 310003, China
[b] Chair of Biological Imaging at the Central Institute for Translational Cancer Research (TranslaTUM), School of Medicine and Health, Technical University of Munich, Munich 81675, Germany
[c] Institute of Biological and Medical Imaging, Helmholtz Zentrum München, Neuherberg 85764, Germany
[d] Institute of Medicinal Chemistry, Helmholtz Zentrum München (GmbH), Neuherberg 85764, Germany
[e] Institute of Structural Biology, Helmholtz Zentrum München (GmbH), Neuherberg 85764, Germany
[f] School of Control Science and Engineering, Shandong University, Jinan 250061, China
[g] Bavarian Center for Biomolecular Mass Spectrometry (BayBioMS), Technical University of Munich, Freising 85354, Germany
[h] Research Unit Analytical Pathology, Helmholtz Zentrum München, Neuherberg 85764, Germany
[i] Bavarian NMR Center, Department of Bioscience, TUM School of Natural Sciences, Technical University of Munich, 85747 Garching, Germany
[j] Center for Biomolecular Drug Research (BMWZ), Institute of Organic Chemistry, Leibniz Universität Hannover, Hannover 30167, Germany

ARTICLE INFO

Keywords:
Cyanine
Barbiturate functionalization
Nanoformulation
NIR-II excitation
Optoacoustic
Photothermal therapy

ABSTRACT

Cyanine derivatives are organic dyes widely used for optical imaging. However, their potential in longitudinal optoacoustic imaging and photothermal therapy remains limited due to challenges such as poor chemical stability, poor photostability, and low photothermal conversion. In this study, we present a new structural modification for cyanine dyes by introducing a strongly electron-withdrawing group (barbiturate), resulting in a new series of barbiturate-cyanine dyes (BC810, BC885, and BC1010) with suppressed fluorescence and enhanced stability. Furthermore, the introduction of BC1010 into block copolymers (PEG_{114}-b-PCL_{60}) induces aggregation-caused quenching, further boosting the photothermal performance. The photophysical properties of nanoparticles (BC1010-NPs) include their remarkably broad absorption range from 900 to 1200 nm for optoacoustic imaging, allowing imaging applications in NIR-I and NIR-II windows. The combined effect of these strategies, including improved photostability, enhanced nonradiative relaxation, and aggregation-caused quenching, enables the detection of optoacoustic signals with high sensitivity and effective photothermal treatment of *in vivo* tumor models when BC1010-NPs are administered before irradiation with a 1064 nm laser. This research introduces a barbiturate-functionalized cyanine derivative with optimal properties for efficient optoacoustics-guided theranostic applications. This new compound holds significant potential for biomedical use, facilitating advancements in optoacoustic-guided diagnostic and therapeutic approaches.

1. Introduction

Light-triggered theranostics is an exciting approach for cancer imaging and treatment, offering non-invasive, spatially controllable methods with minimal systemic toxicity [1–5]. This strategy primarily utilizes near-infrared (NIR) light to activate photothermal agents, generating localized heat for optoacoustic (OptA) detection and photothermal therapy (PTT) [2,6–8]. Recently, significant progress has been

* Corresponding authors at: Chair of Biological Imaging at the Central Institute for Translational Cancer Research (TranslaTUM), School of Medicine and Health, Technical University of Munich, Munich 81675, Germany.
E-mail addresses: vipul.gujrati@tum.de (V. Gujrati), bioimaging.translatum@tum.de (V. Ntziachristos).

https://doi.org/10.1016/j.jconrel.2024.06.037
Received 1 March 2024; Received in revised form 13 June 2024; Accepted 16 June 2024
Available online 27 June 2024

made in the development of various synthetic agents enabling efficient photothermal theranostics [2]. In particular, agents with absorption in the NIR range have garnered attention for deep-tumor theranostics, as they exhibit minimal phototoxicity and reduced background noise caused by water and hemoglobin absorption [9,10]. However, concerns regarding the long-term safety profiles of inorganic agents for clinical use remain unanswered [7,11]. In this context, organic dyes present notable advantages due to their superior biocompatibility, higher biodegradability, and existing FDA approvals [12–14].

Cyanine dyes, composed of polymethine chains with conjugated nitrogen atoms enclosed in N-heterocyclic ring systems, are widely employed in biomedical imaging and are commercially available [15,16]. Indocyanine green (ICG), an FDA-approved cyanine derivative, has been applied clinically for fluorescence imaging due to its structural biosafety [17,18]. Due to their strong and narrow absorption peak in the NIR region, cyanine dyes are used in OptA imaging to achieve high contrast. However, their application in longitudinal OptA imaging and PTT is limited due to poor photostability, low photothermal conversion, and inefficient OptA generation. Additionally, cyanine dyes tend to aggregate in aqueous solutions and their optical properties are influenced by the microenvironment [19].

Several molecular design strategies have been explored to enhance the OptA and photothermal performance of cyanine derivatives [20]. Quenching intersystem crossing in cyanine structures has been achieved by bridging triplet-state quencher moieties, ensuring stable OptA output by reducing singlet oxygen ($^1O_2$) generation that affects dye photostability [21]. Furthermore, the construction of a photoinduced electron transfer system at the meso-position of cyanine has been demonstrated to quench fluorescence and enhance photothermal performance [22]. Additionally, strong intramolecular charge transfer states have been developed to enhance the nonradiative heat of cyanine [23]. However, these molecular structures often involve long-branched alkyl chains and bulky substituents to support molecular motion in aggregates. Hence, there is an ongoing need for novel synthetic approaches to develop cyanine dyes that possess enhanced photothermal properties. Such advancements would greatly contribute to the effectiveness of cyanines for *in vivo* OptA applications.

To overcome these challenges, we propose incorporating a strong electron-withdrawing group (EWG) at the meso-position of cyanine structures, thereby effectively suppressing fluorescence, enhancing nonradiative decay, and improving photostability [24,25]. Barbiturate, a bulky and electron-withdrawing substitute commonly found in merocyanine dyes, offers structure rigidification and facilitates electron-transfer when cross-conjugated within the cyanine framework [26–29]. In this study, we synthesized a new set of barbiturate-cyanine dyes (specifically BC810, BC885, and BC1010), and analyzed their optical properties before nanoformulating them for use in OptA applications inside the body. Among the derivatives, BC1010 showed the best stability in water, making it the chosen candidate for further testing in mouse OptA imaging. For *in vivo* applications, BC1010 was nanoformulated into nanoparticles (BC1010-NPs) and further characterized by size, stability, and their optical properties, taking into account the aggregation-caused quenching effect. We evaluated the OptA performance of BC1010-NPs in tissue-mimicking phantoms and two tumor models (4T1 breast cancer and HCT116 orthotopic colon cancer). Additionally, we characterized and verified the photothermal profile of BC1010-NPs in *in vitro* and *in vivo* cancer models. Biosafety studies were conducted by assessing blood parameters and histology in mouse models. This study introduces new cyanine-based nanoagents for sensitive OptA detection and efficient tumor elimination through PTT.

2. Materials and methods

2.1. Materials

All chemical reagents were purchased from abcr GmbH (Germany). PEG_{114}-b-PCL_{60} was ordered from Advanced Polymer Materials Inc. (Montreal, Canada). The MTT assay kit and 1,3-Diphenylisobenzofuran (DPBF) were purchased from Sigma-Aldrich (Germany). Calcein-acetoxymethyl (AM) and ethidium homodimer-1 (EthD1) were bought from Thermo Fisher Scientific.

2.2. Synthesis of BC810, BC885, BC1010

*5-((2E,5E)-2,5-bis((dimethylamino)methylene)cyclopentylidene)-1,3-dimethylpyrimidine-2,4,6(1H,3H,5H)-trione **XX**.*

Enamine **XX** was prepared according to a patented procedure [30] and was obtained as a bright orange powder (3.77 g, 19% yield after 4 steps). **^{1}H NMR** (400 MHz, DMSO-d_6) δ 7.05 (s, 2H), 3.16 (s, 12H), 3.05 (s, 6H), 2.96 (s, 4H). **^{13}C NMR** (101 MHz, DMSO-d_6) δ 179.16, 160.68, 152.86, 151.68, 117.33, 80.05, 42.84, 28.27, 26.97. HRMS (ESI$^+$): calcd. for $C_{17}H_{29}N_4O$: $[M + H]^+ = 305.2341$, found: $[M + H]^+ = XX$.

*1,3-dimethyl-5-((2E,5E)-2-((E)-2-(3-methylbenzo[d]thiazol-2(3H)-ylidene)ethylidene)-5-((Z)-2-(3-methy)lbenzo[d]thiazol-2(3H)-ylidene)ethylidene)cyclopentylidene) pyrimidine-2,4,6(1H,3H,5H)-trione (**BC810**).*

A stirred mixture of 2,3-dimethylbenzo[*d*]thiazol-3-ium iodide [31] (102 mg, 0.351 mmol) and enamine XX (58 mg, 0.177 mmol) were dissolved in dry acetonitrile (5 mL) and heated to 120 °C for 2 h in a CEM microwave reactor. After cooling to room temperature, the crude product was filtered and washed with methanol to give BC810 as a black solid (48 mg, 48%). **^{1}H NMR** (500 MHz, DMSO-d_6) δ 7.82 (d, $J = 7.9$ Hz, 2H), 7.54 (d, $J = 8.4$ Hz, 2H), 7.46 (t, $J = 7.8$ Hz, 2H), 7.26 (t, $J = 7.6$ Hz, 2H), 7.13 (d, $J = 13.2$ Hz, 2H), 6.07 (d, $J = 13.3$ Hz, 2H), 3.73 (s, 6H), 3.15 (s, 6H), 2.78 (s, 4H). **MALDI-TOF**: $m/z = 570.203$.

*5-((2E,5E)-2,5-bis((Z)-2-(1-benzylbenzo[cd]indol-2(1H)-ylidene)ethylidene)cyclopentylidene)-1,3-dimethylpyrimidine-2,4,6(1H,3H,5H)-trione (**BC885**).*

A stirred mixture of 1,2-dimethylquinolin-1-ium iodide [32] (156 mg, 0.54 mmol) and enamine XX (90 mg, 0.28 mmol) was dissolved in dry acetonitrile (5 mL) and heated to 120 °C for 2 h in a microwave reactor. After cooling to room temperature, the crude product was filtered and washed with methanol to give BC885 as a black solid (29 mg, 19%). **MALDI-TOF**: $m/z = 556.13$.

*5-((2E,5E)-2,5-bis((Z)-2-(1-benzylbenzo[cd]indol-2(1H)-ylidene)ethylidene)cyclopentylidene) -1,3-dimethylpyrimidine-2,4,6(1H,3H,5H)-trione (**BC1010**).*

A stirred mixture of 1-benzyl-2-methylbenzo[*cd*]indol-1-ium iodide [30] (359 mg, 0.931 mmol) and enamine XX (141 mg, 0.424 mmol) was dissolved in dry acetonitrile (4 mL) and heated to reflux for 2 h over an argon atmosphere. After cooling to room temperature and filtering, the crude solid was washed with methanol to afford BC1010 as a black solid (298 mg, 92%). Due to low solubility, further purification could only be accomplished in small amounts. Silica gel chromatography on a 30 mg sample eluted with DCM/MeOH 95:5 afforded pure product with an $R_f = 0.5$. **MALDI-TOF**: $m/z = 757.494$.

2.3. Synthesis of BC1010-NPs

The nanoformulation procedures of BC1010 were prepared as previously described [33]. BC1010 (3 mg) and PEG_{114}-b-PCL_{60} (12 mg) were dissolved in DMSO (1.5 mL). The mixture was then added dropwise into 15 mL deionized water under continuous (for 10 min) sonication, followed by another 2 h of stirring. The obtained BC1010-NPs were filtered through a 400 nm syringe filter and then concentrated with a centrifugal filter (MWCO = 100 kDa) for further use.

2.4. Characterization

The m/z ratios of the compounds were recorded with a MALDI UltrafleXtreme (Bruker) using dihydroxybenzoic acid as the matrix. The morphology of BC1010-NPs was obtained by transmission electron microscopy (TEM) (Zeiss Libra 120 Plus, Carl Zeiss NTSb GmbH, Germany)

with the setting of a bright-field image model. The particle size distribution of BC1010-NPs was measured using 50 μg/mL in water or 10% FBS, using Malvern Zetasizer. Absorption spectra were recorded with a SHIMADZU UV-3600 Plus UV-Vis-NIR spectrometer. Relative quantum yields were measured with a steady state and time-resolved photoluminescence spectrometer (Edinburg FLS1000) [34]. OptA spectra of BC1010-NPs were measured in D_2O using a MSOT inVision 256-TF (iThera Medical, Munich, Germany) which was normalized with India ink [35]. The OptA stability of samples was evaluated by pulsed laser irradiation from the MSOT inVision 256-TF (fluence 10 mJ/cm^2) for 60 min.

2.5. In vitro penetration depth estimation

A mixture of India ink solution (98 mL, absorbance 0.15 at 780 nm), intralipid (2 mL), and agar (2 g) was used to prepare the tissue-mimicking cylindrical phantoms with different radii (4, 7, 9, 12 mm). Tubing containing BC1010-NPs at various concentrations was separately inserted into the center of these agar phantoms and was then imaged using an MSOT inVision 256-TF with multiple wavelengths. The image contrast was calculated by $(OptA_{sig} - OptA_{bg})/(OptA_{sig} + OptA_{bg})$, where $OptA_{bg}$ and $OptA_{sig}$ were the mean OptA intensities of the agar phantom and sample (BC1010-NPs) at the various wavelengths, respectively [36].

2.6. In vivo OptA imaging of various tumor models

Procedures involving animal experiments were approved by the Government of Upper Bavaria, and Animal Care and Use Committee of the First Affiliated Hospital, Zhejiang University School of Medicine. The 4T1 subcutaneous tumor model was prepared using 6-week-old nude mice by subcutaneously implanting 4T1 cells (1×10^6 cells in 30 μL PBS) on the back of these mice. The *in vivo* OptA imaging and further PTT were carried out when the tumor volume reached 100 mm^3. An orthotopic colon tumor model was also developed using 6-week-old nude mice ($n = 3$) by intraperitoneally injecting HCT116 cells (3×10^6 cells in 100 μL PBS) and imaging after two weeks. For better visualization, a MSOT inVision 256-TF with an extended laser wavelength (up to 1300 nm) was used. Heavy water was filled into the tank for animal scanning. The *in vivo* OptA images were acquired before and after intravenous (i.v.) injection of 100 μL BC1010-NPs (3 mg/mL) with multiple wavelengths (975, 1045, 1064, 1100, 1160, 1210, 1230 nm) scanned. Here, the pre-scan (before treatment) images are considered as untreated controls. The image reconstruction was performed using a "model linear" approach using ViewMSOT 4.0 software (iThera Medical, Munich). The spectral unmixing method (linear regression) was used to unmix the signal of BC1010-NPs from H_2O and HbO_2 at the scanned wavelengths.

2.7. In vitro photothermal effect of BC1010-NPs

The photothermal performance of BC1010-NPs was evaluated by recording temperature increases in solutions with varying concentrations of BC1010-NPs during irradiation using a 1064 nm continuous wave (CW) laser at various power settings. The following equation was used to calculate the photothermal conversion efficiency (PCE) of BC1010-NPs: $\eta = [(hS(T\text{-}T_{surr})\text{-}Q_{Dis}]/I(1\text{–}10^{-A1064})$, where the 1064 nm continuous wave (CW) laser power (I) was 0.8 W/cm^{2,} and the absorbance of the BC1010-NPs solution at 1064 nm was 0.549 at 1064 nm [37]. The photothermal treatment for deep tissue was mimicked by covering a BC1010-NP sample with different thicknesses of chicken breast tissue and then evaluating the temperature changes of BC1010-NPs solutions during laser irradiation.

4T1 cells were seeded in a 96-well plate overnight (1×10^4 cells/well) and then treated with different concentrations of BC1010-NPs for 24 h to test the nanoparticles' toxicity. The laser-treated group was irradiated (1064 nm CW laser, for 5 min) after 4 h of co-incubation with BC1010-NPs. Cell viability was assessed by MTT assay. Live/dead cell assays were used to visualize the photothermal effect of BC1010-NPs at the cell level by co-staining with Calcein-AM and EthD-1 for 30 min, followed by PBS washing and fluorescence imaging using a Leica DMI3000 B Inverted Microscope (Wetzlar, Germany).

2.8. In vivo PTT of 4T1 tumor-bearing mice

4T1 tumor-bearing mice with around 100 mm^3 tumor volume were randomly divided into four groups ($n = 3$ per group) and the following treatments were performed: PBS, BC1010-NPs, PBS + laser, and BC1010-NPs + laser. In the laser-treated groups, the tumor region was irradiated with a 1064 nm CW laser at 0.8 W/cm^2 for 10 min after i.v. injection of PBS or BC1010-NPs (100 μL, 3 mg/mL) four hours earlier. A thermal infrared camera recorded the temperature of tumor areas in mice from the laser-treated groups. Tumor growth was monitored through daily caliper measurements. The body weights of mice were measured until 8 days after treatment. On the last day of the study, the mice were sacrificed, and the vital organs and tumors from each group were collected and examined by H&E staining.

2.9. In vivo biosafety evaluation of BC1010-NPs

Immune-competent C57BL/6 mice were randomly separated into 4 groups ($n = 5$ per group) to evaluate biosafety *in vivo* [38]. Mice in three of the groups were i.v. injected with 100 μL BC1010-NPs (3 mg/mL), and their blood was collected on days 1, 7, and 14. The control group was treated with 100 μL PBS, and blood was collected on day 14. Blood biochemistry and hematology were examined in the collected blood using a Hitachi 917 Clinical Chemistry Analyzer (Roche, Germany). The vital organs from these 4 groups were isolated and evaluated by means of H&E staining.

2.10. Statistical analysis

Statistical analysis was performed using OriginPro 8. Inter-group differences were assessed for significance using One-Way/Two-Way ANOVA with Tukey's HSD test. Results were expressed as mean ± SD, and differences were considered significant if $P < 0.05$.

3. Results and discussion

3.1. Synthesis and characterization of barbiturate cyanines

Barbiturate-cyanines (BC810, BC885, and BC1010) were synthesized by condensation of suitably functionalized iminium salts with a barbituric acid enamine core (Fig. 1a, Fig. S1, S2). After simple filtration, the dyes were found to be pure by thin-layer chromatography and had MALDI-TOF mass spectra consistent with their proposed structures (Fig. S3). With the exception of BC810 (Fig. S4), obtaining satisfactory NMR spectra proved challenging due to low solubility (in deuterated DMSO, pyridine, and chloroform), and the existence of multiple conformers of BC885 and BC1010 on the NMR timescale. Measurement at elevated temperature (60 °C in DMSO) was not sufficient to result in an optimally resolved spectrum, and we found that other authors have observed similar problems with very similar compounds [39,40]. The absorption spectra for BC810, BC885, and BC1010 were measured in dichloromethane (DCM) and strong absorption peaks occurred at 810, 885, and 1010 nm (Fig. 1b), respectively. Furthermore, these three derivatives exhibited high molar absorption coefficient and low fluorescent quantum yield (Table S1), especially BC1010, which exhibited a quantum yield of around 60% less than IR1048. Next, density functional theory (DFT) calculations were performed using the Gaussian 16 program package [41]. The highest occupied molecular orbitals (HOMO) were found to be distributed over the conjugated structure while the lowest unoccupied molecular orbitals (LUMO) were localized on the

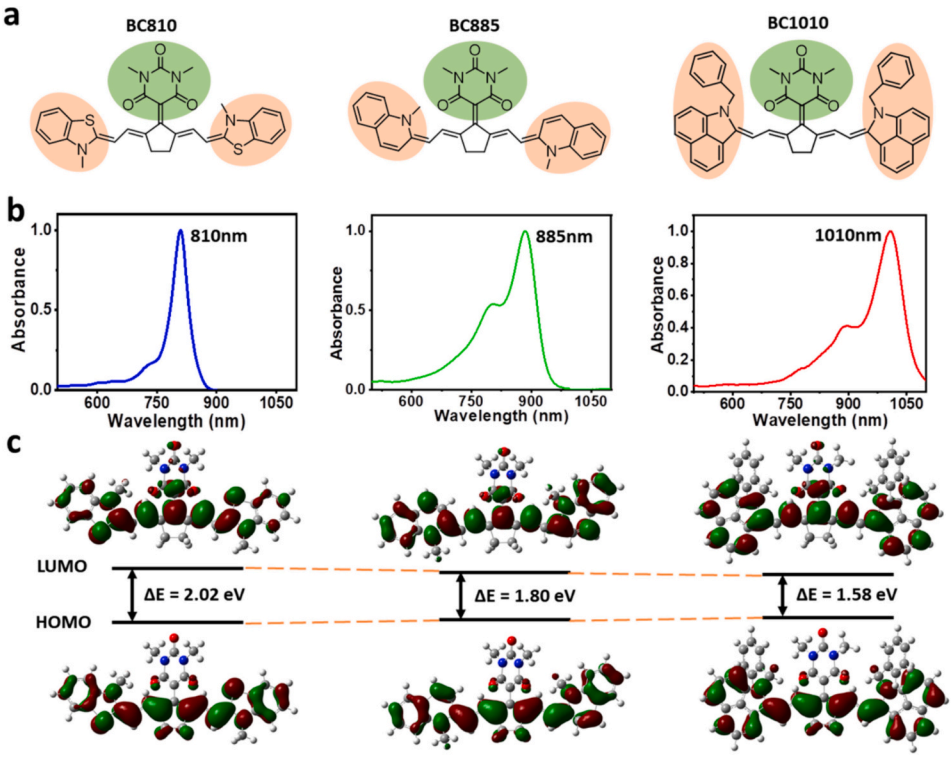

Fig. 1. Structure and physical characterization of barbiturate cyanines (BCs). The (a) structures and (b) absorption spectra of BC810, BC885, and BC1010 in dichloromethane (DCM). (c) Calculated highest occupied molecular orbital-lowest occupied molecular orbital (HOMO-LUMO) energy gap of BC810, BC885, and BC1010 with optimized geometry at the B3LYP/def2-SVP level in DCM.

acceptor barbiturate motif, suggesting a charge-transfer characteristic of the dyes. The bandgaps of BC810, BC885, and BC1010 were calculated to be 2.02, 1.80, and 1.58 eV, respectively (Fig. 1c). These tapering bandgaps were in agreement with the absorption bathochromic shift trend. Surprisingly, we found that BC810 and BC885 became rapidly bleached, IR1048 blue shifted under aqueous conditions, while BC1010 maintained its absorption characteristics under the same conditions (Fig. S5). Therefore, we considered BC1010 the most suitable for further OptA/PTT bio-applications.

3.2. Fabrication and characterization of BC1010-NPs

To improve the *in vivo* bioavailability of hydrophobic BC1010, we employed PEG_{114}-b-PCL_{60} to formulate a nano-aggregate (BC1010-NPs) through a nanoprecipitation process (Fig. 2a). The developed BC1010-NPs were first characterized by their particle dimensions. Transmission electron microscopy (TEM) and dynamic light scattering (DLS) showed that the aggregates had an average diameter of ~125 nm (Fig. 2b). Importantly, BC1010-NPs maintained a similar size distribution in water and 10% fetal bovine serum (FBS) for 14 days, suggesting good stability (Fig. 2c). Next, we tested the optical properties of BC1010-NPs. The nano-aggregate spectrum exhibits a remarkably broad absorption range from 900 to1200 nm with completely quenched fluorescence, which is attributed to the self-aggregation of the dye (Fig. 2d, e). And BC1010-NPs have more stable absorption than BC1010 dye during 24 h's observation (Fig. S6). Considering the possible photodynamic effect from BC1010-NPs during laser irradiation, 1,3-Diphenylisobenzofuran (DPBF) was used to test their $^1O_2$ generation. No decrease of DPBF absorbance indicates the lack of photodynamic effect from BC1010-NPs (Fig. S7). These results indicate that BC1010-NPs efficiently absorb laser energy and generate strong heat rather than following dissipative pathways (fluorescence or intersystem crossing). The OptA signal of BC1010-NPs was measured in the D_2O-filled MSOT setup, where the normalized OptA spectrum showed similarity with the absorption spectrum (Fig. 2f). We also continuously monitored the OptA intensity of BC1010 and BC1010-NPs following 60 min of pulsed laser irradiation. The unbleached signal suggested excellent photostability of BC1010 and BC1010-NPs compared to ICG (Fig. 2g, Fig. S8).

3.3. In vitro OptA imaging of BC1010-NPs at different depths

To verify deep tissue imaging capacity using BC1010-NPs, tissue-mimicking cylindrical agar phantoms with different thicknesses were employed to examine the OptA signals [42,43]. A tube containing a BC1010-NPs solution was inserted into the center of the agar phantom and then scanned by the MSOT system with multiple wavelengths. Fig. 3a shows lower noise signals from the agar phantoms at the longer wavelength of 1064 nm tested. Image contrast was then used to determine the imaging performance and we found that higher image contrast was observed at 1064 nm even at different depths (Fig. 3b). Additionally, different concentrations of BC1010-NPs were used and the OptA signals detected in phantoms with different thicknesses allowed conclusions to be drawn about the sensitivity of detection at multiple depths (Fig. 3c, Fig. S9). A comparison between dye and nanoparticles indicated that the signal generated by BC1010-NPs was stronger than BC1010 dye (S10). These results suggest that BC1010-NPs can be used for effective deep-tissue imaging.

3.4. In vivo OptA imaging with BC1010-NPs

Encouraged by the strength and stability of OptA signals from phantoms, we confirmed the suitability of BC1010-NPs for *in vivo* applications by imaging a 4T1 subcutaneous breast tumor and orthotopic colon tumor. As shown in Fig. 4a, the unmixed OptA images of 4T1 tumor-bearing mice were captured at different time points (pre-injection, 1 h, 4 h, 8 h, 12 h, and 24 h post-BC1010-NPs injection). Free BC1010 dye showed minimal tumor accumulation, likely due to rapid clearance (Fig. S11), but the nanosized BC1010-NPs displayed a gradual

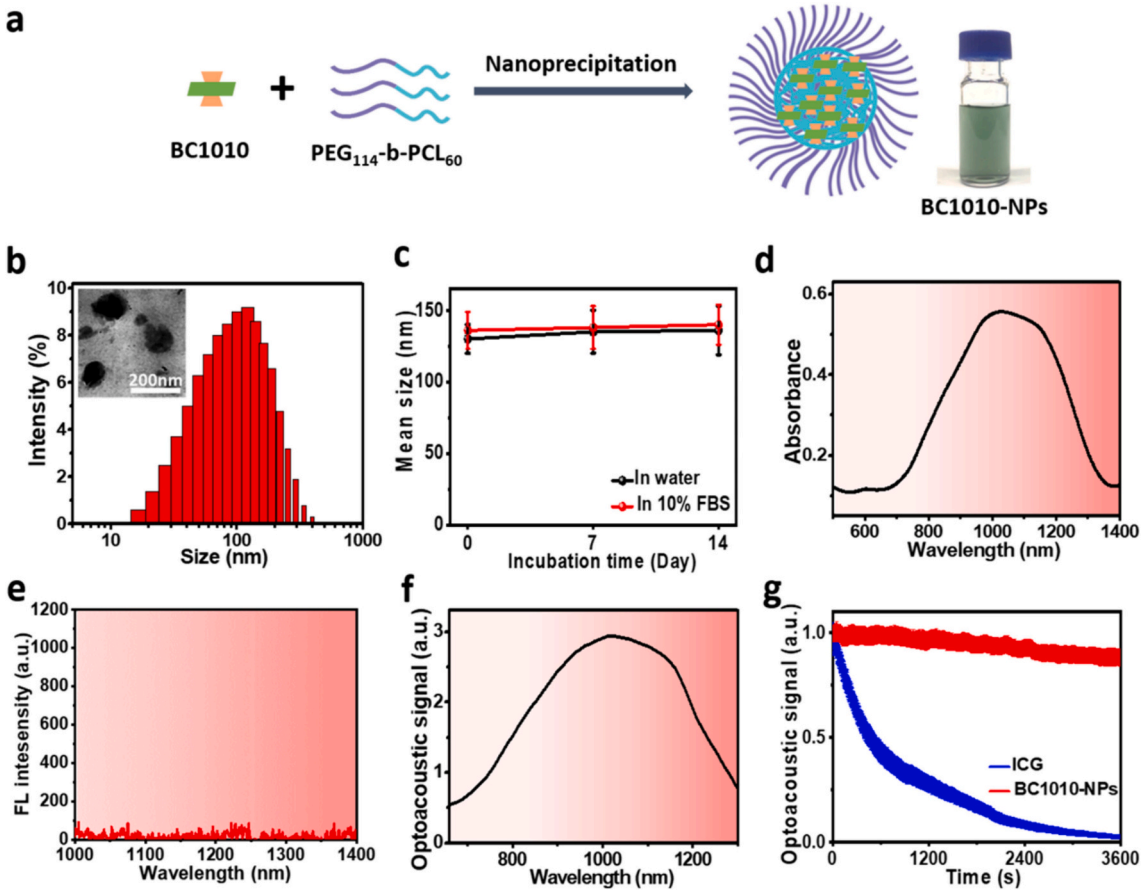

Fig. 2. Physical characterization of BC1010-NPs. (a) The synthetic scheme of BC1010-NPs using a nanoprecipitation method. (b) Transmission electron microscopy (TEM) image and dynamic light scattering (DLS) profile of BC1010-NPs. (c) The average size distribution of BC1010-NPs (50 μg/mL) in water or 10% FBS over 14 days of incubation. (d) Optical spectrum, (e) Fluorescence intensity (1000 nm - 1400 nm) and (f) OptA spectrum of BC1010-NPs. (g) OptA signal stability of BC1010-NPs and ICG (in 10%FBS) after 60 min of pulsed laser irradiation (fluence 10 mJ/cm^2).

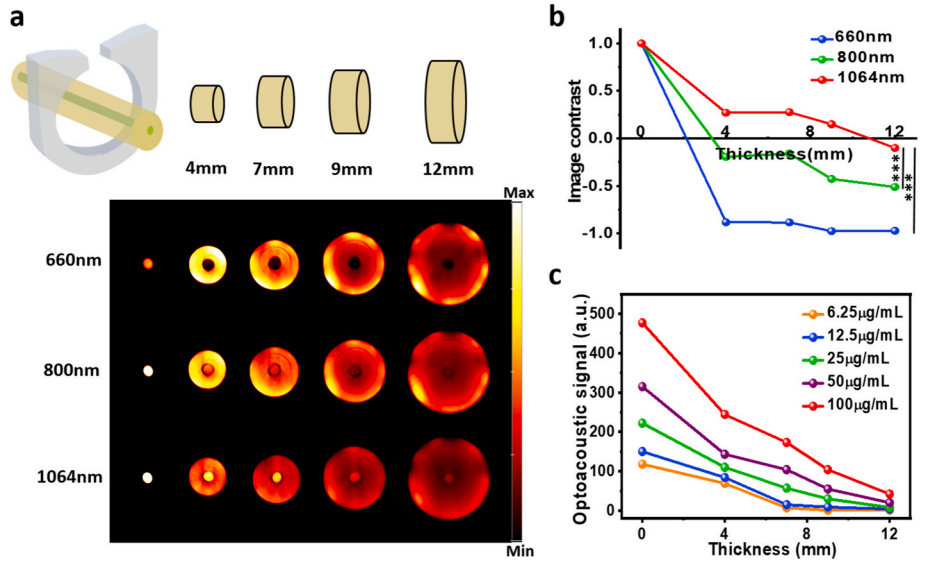

Fig. 3. Optoacoustic (OptA) imaging with BC1010-NPs *in vitro*. (a) OptA images of cylindrical tissue-mimicking phantoms, with different radii containing BC1010-NPs (100 μg/mL) in the center, captured at different wavelengths. (b) Image contrast of BC1010-NPs (100 μg/mL) in phantoms of different thicknesses at different wavelengths. (c) OptA signals from various concentrations of BC1010-NPs in tissue-mimicking cylindrical phantoms with different radii.

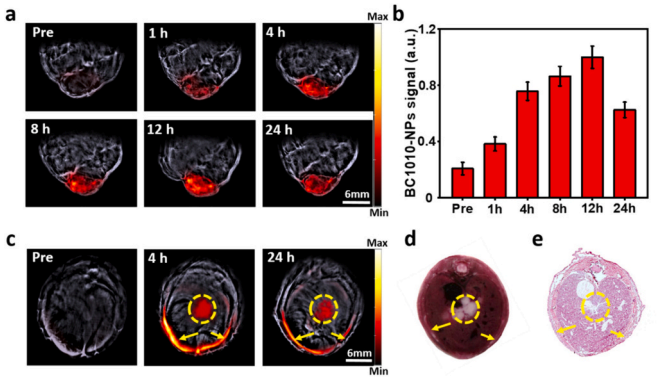

Fig. 4. Optoacoustic (OptA) imaging with BC1010-NPs *in vivo*. (a) Representative unmixed multispectral optoacoustic tomography (MSOT) images of a 4T1 subcutaneous tumor model after intravenous injection of BC1010-NPs (100 μL, 3 mg/mL) ($n = 3$). The red color in the tumor regions indicates signal from the unmixed BC1010-NPs. (b) Quantitated OptA signals from tumor areas at various time points. (c) Representative unmixed images of a HCT116 orthotopic colon tumor after intravenous injection of BC1010-NPs (100 μL, 3 mg/mL) (n = 3). (d, e) Bright-field image and image of hematoxylin and eosin (H&E)-stained colon tumor cryosection (yellow arrows and circle indicate the tumor locations). (For interpretation of the references to color in this figure legend, the reader is referred to the web version of this article.)

signal increase in the tumor region over time with a maximum accumulation at around 12 h post-injection because of the enhanced permeability and retention (EPR) effect. When the imaging time was extended to 24 h, the OptA signal from the tumor showed a partial decrease, indicating systemic clearance of BC1010-NPs from the tumor region. The quantitative measurements also showed higher tumor enrichment of BC1010-NPs at 4–12 h post-injection, suggesting the optimal time points for PTT (Fig. 4b).

Fig. 4c shows representative OptA images of orthotopic colon tumors pre-injection, 4 h and 24 h post BC1010-NPs injection. MSOT images of colon tumors displayed enhanced OptA signal from the enterocoelic wall. More specifically, the colon tumor localized at the center of the mouse body was visualized, indicating that the laser light could reach deeper tissues and thus could produce OptA signals from the tumor upon light absorption by BC1010-NPs. In addition, images of hematoxylin and eosin (H&E)-stained cryosections confirmed the presence of colon tumors at the corresponding positions (Fig. 4d, e). These results prove that BC1010-NPs enabled visualization of deep-seated tumors using an OptA imaging system.

After 24 h post-injection of BC1010-NPs, the tumors and vital organs (kidney, liver, spleen, heart) from the two tumor models were resected to examine *ex vivo* biodistribution of BC1010-NPs. The higher liver OptA signals from the coronal plane images were likely due to hepatic clearance (Fig. S12). In addition, the blood clearance profile of BC1010-NPs was analyzed by measuring BC1010-NPs concentrations in blood collected at various time points post-injection. The clearance half-life was calculated to be ~10 h (Fig. S13).

3.5. In vitro PTT of BC1010-NPs

Inspired by the strong absorption in the extended NIR window, BC1010-NPs were tested for heat generation and suitability for PTT. To assess the photothermal performance of BC1010-NPs, a 1064 nm continuous wave (CW) laser was used to irradiate different concentrations of BC1010-NPs with various laser powers while recording the temperatures of the samples. As shown in Fig. 5a and b, the temperature rise attributed to irradiated BC1010-NPs showed a clear correlation with the employed BC1010-NPs concentration and laser power densities. Specifically, within 2 min of laser irradiation (0.8 W/cm^2), the 100 μg BC1010-NPs /mL solution displayed a rapid temperature increase of ~15 °C, while water only had a ~ 3 °C increase under the same condition. We calculated the photothermal conversion efficiency (PCE) of BC1010-NPs based on the temperature cooling curve, and obtained an average value of ~38.5% (Fig. 5c). In addition, Fig. 5d shows the excellent photothermal stability of BC1010-NPs under four cycles of laser irradiation.

To evaluate the photothermal effect in deep tissue, we first investigated the residual power densities of a 780 nm and a 1064 nm CW laser after penetrating different thicknesses of chicken breast tissue (Fig. 5e and f). Fig. 5f showed that the residual power intensities of the 780 nm CW laser were diminished rapidly at each tissue depth compared with the 1064 nm CW laser. This is attributed to the better transmittance capability of tissue at 1064 nm compared with the shorter wavelengths.[29] Next, a BC1010-NPs solution (100 μg/mL) was placed under chicken breast tissue of increasing thicknesses to measure the temperature increase of BC1010-NPs solutions after irradiation with a 1064 nm CW laser. BC1010-NPs exhibited temperature increases of ~12 °C, 10 °C, and 8 °C at 4 mm, 6 mm, and 8 mm depths (Fig. 5g). These changes at such deep depths indicate the high clinical translation potential for PTT of deep tumors.

Since heating to 42–45 °C for 5 min can induce killing of cancerous cells [44], we further evaluated the photothermal effect of BC1010-NPs in 4T1 breast cancer cells by a standard MTT cell viability assay. Fig. 5h demonstrated the negligible cytotoxicity of BC1010-NPs after 24 h of incubation, while the apparent photothermal toxicity of BC1010-NPs upon laser irradiation was significantly higher. Specifically, 100 μg/mL of BC1010-NPs treatment induced ~90% cell death after 5 min of laser exposure. Besides using an MTT assay, cell death was also visualized using a live/dead cell assay, which showed remarkable differences in cellular cytotoxicity (Fig. 5i and Fig. S14).

3.6. In vivo PTT using BC1010-NPs

To validate *in vivo* tumor PTT with BC1010-NPs, we randomly divided 4T1 tumor-bearing mice into four treatment groups: PBS, PBS + laser, BC1010-NPs, and BC1010-NPs + laser. After considering our results on BC1010-NPs accumulation in tumors and the relevant *in vivo* OptA images, the laser-treated groups were irradiated 4 h after i.v. injection of PBS or BC1010-NPs. A thermal camera was used to monitor the temperature changes of tumor areas during the 10 min of irradiation. Fig. 6a, b displays a mild temperature increase in the PBS + laser group and a rapid temperature rise (up to ~49.8 °C) in the BC1010-NPs + laser group, which is enough to induce cell death in cancer cells [44–46].

After the indicated treatments, the tumor volumes and body weights of mice were continuously monitored for eight days. As demonstrated in Fig. 6c, d, the mice subjected to BC1010-NPs + laser showed significant tumor growth suppression, while the other three control groups displayed rapid tumor growth. The bioluminescence imaging of 4T1-Luc tumor bearing mice further confirmed the efficient anti-tumor effect upon the treatment of BC1010-NPs + Laser (Fig. S15). These results implied that BC1010-NPs treatment with 1064 nm-laser irradiation could produce an immense amount of heat for killing cancerous cells. Moreover, the photothermal effect was validated by examination of H&*E*-stained sections from the tumor areas after 8 days of treatments. Cell shrinkage and necrosis can be seen in the sections from the BC1010-NPs + laser group, while typical pathological features of cancer can be seen in sections from the control groups, such as eosinophilic intranuclear inclusion bodies and an increased karyoplasmic ratio (Fig. 6f) [47]. In addition, the safety of the treatment was assessed by monitoring body weight of the mice and H&E staining of sections from the vital organs. No noticeable changes in body weights (Fig. 6d) and no pathological tissue damage (Fig. S16) were observed, which suggest that BC1010-NPs are highly biocompatible.

Furthermore, healthy C57BL/6 mice were used to confirm safety of BC1010-NPs through blood testing and histological examination of organ samples. There were no significant differences between the

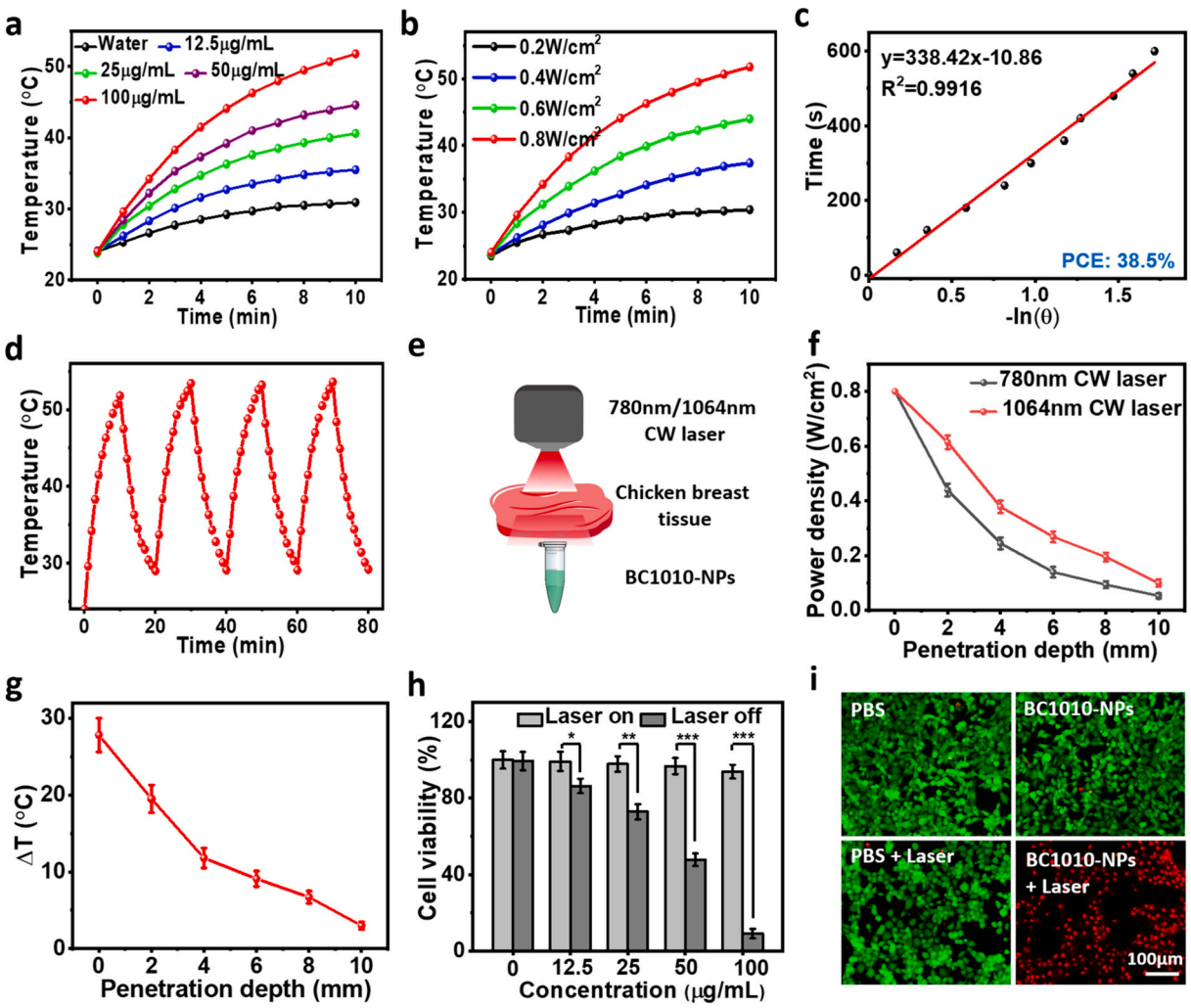

Fig. 5. The photothermal effect of BC1010-NPs *in vitro*. (a) Temperature change curves of various BC1010-NPs solutions upon 1064 nm continuous wave (CW) laser irradiation (0.8 W/cm^2). (b) Temperature change curves of a BC1010-NPs solution (100 μg/mL) upon exposure to a 1064 nm CW laser with various powers. (c) Linear correlation of the cooling times of BC1010-NPs *versus* the negative logarithm of temperature. (d) Temperature changes of a BC1010-NPs (100 μg/mL) solution during four cycles of alternating heating (10 min) and cooling (10 min). (e) Schematic illustration of deep-tissue PTT model. (f) After passing through chicken breast tissue with increasing depths, residual power densities of the 780 nm and 1064 nm CW laser are shown ($n = 3$). (g) Temperature changes of BC1010-NPs (100 μg/mL) solutions covered with various thicknesses of chicken breast tissue upon 10 min laser irradiation (1064 nm CW laser, 0.8 W/cm^2) (n = 3). (h) Relative viabilities of 4T1 cells after treatment with BC1010-NPs in the absence or presence of a 1064 nm CW laser irradiation (0.8 W/cm^2, 5 min). (i) Live/dead stained images of 4T1 cells with the indicated treatments. Calcein-AM (green color) and EthD-1 (red) staining indicate live and dead cells respectively. (For interpretation of the references to color in this figure legend, the reader is referred to the web version of this article.)

control and BC1010-NPs treated groups on different days when blood hematology, blood biochemistry, and H&E images of major organs were compared, suggesting no toxic side effects from BC1010-NPs (Fig. S17). Altogether, these results indicated that BC1010-NPs were efficacious for tumor PTT and exhibited good biocompatibility.

4. Discussion

This study presents a strategy for the generation of cyanine derivatives that exhibit improved photophysical and photochemical properties compared to ICG, specifically optimized for OptA applications. The introduction of barbiturate, a strong EWG at the meso-position of the cyanine structures, and the cross-conjugated arrangement of the barbiturate cyanine structure induced electron-transfer, significantly decreases fluorescence and leads to decreased ROS formation upon radiation, resulting in a robust photothermal conversion effect and an increased stability of the dye. Additionally, the bulky substituent barbiturate enhances the structural rigidification of cyanines, further contributing to good photostability. While all three derivatives (BC810, BC885, and BC1010) feature a conjugated system, BC810 and BC885 showed reduced absorption in water, but BC1010 displayed excellent water stability. Possibly, BC1010's very hydrophobic nature resulted in a higher surface tension and formation of non-wettable aggregates, making it unreactive towards water. The nano-formulation method employed in this study not only improves the water stability of BC1010 and provides sufficient solubility for *in vivo* application, but also facilitates complete fluorescence quenching through efficient intramolecular electron transfer. The prepared BC1010-NPs exhibited stable sizes in the nanometer range, complete fluorescence quenching, good photothermal performance, high photostability, enhanced OptA contrast, and low toxicity, making them ideal for biomedical applications. These BC1010-NPs allowed for sensitive OptA detection of deep tumors, including breast and colon cancer. Upon irradiation with a 1064 nm laser, BC1010-NPs generated significant heat, leading to effective cell killing and tumor elimination. Furthermore, BC1010-NPs demonstrated excellent *in vivo* biocompatibility and systemic tolerance. Overall, this study demonstrates the effectiveness of EWG-barbiturate functionalization of cyanines, which can be widely

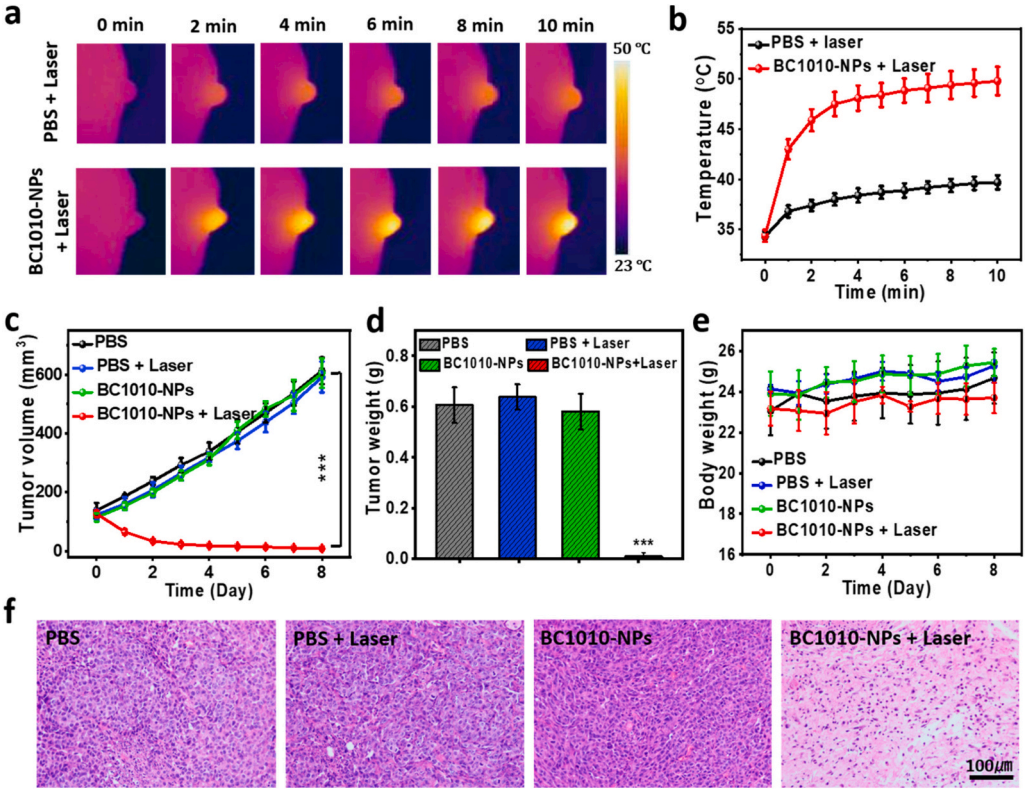

Fig. 6. Photothermal therapy (PTT) using BC1010-NPs *in vivo*. (a) Representative thermal images of 4T1 tumor-bearing mice before and during a 10 min irradiation period with a 1064 nm CW laser (0.8 W/cm^2). Four hours before irradiation, mice were injected intravenously with PBS or BC1010-NPs. (b) Tumor temperatures over time in the two treatment conditions shown in panel a. The (c) relative tumor volumes, (d) tumor weights, and (e) body weights of mice monitored over 8 days after injection of PBS or BC1010-NPs with or without laser irradiation ($n = 3$ per group). (f) Images of hematoxylin and eosin (H&E)-stained tissue sections from the tumor area in the different treatment groups on day 8. (***$p < 0.001$).

applied to develop numerous imaging probes based on cyanine dyes. These findings and proposed approach have broad implications for photothermal theranostics applications.

CRediT authorship contribution statement

Nian Liu: Writing – review & editing, Writing – original draft, Visualization, Validation, Methodology, Formal analysis, Data curation, Conceptualization. **Patrick O'Connor:** Writing – review & editing, Writing – original draft, Visualization, Validation, Methodology, Formal analysis, Data curation, Conceptualization. **Vipul Gujrati:** Writing – review & editing, Writing – original draft, Visualization, Validation, Methodology, Formal analysis, Data curation, Conceptualization. **Divyesh Shelar:** Data curation, Methodology. **Xiaopeng Ma:** Writing – review & editing, Methodology, Formal analysis, Data curation. **Pia Anzenhofer:** Methodology, Data curation. **Uwe Klemm:** Methodology, Data curation. **Xinhui Su:** Data curation, Methodology. **Yuanhui Huang:** Writing – review & editing, Formal analysis, Data curation. **Karin Kleigrewe:** Writing – review & editing, Writing – original draft, Formal analysis, Data curation. **Annette Feuchtinger:** Writing – review & editing, Writing – original draft, Formal analysis, Data curation. **Axel Walch:** Writing – review & editing, Writing – original draft, Formal analysis. **Michael Sattler:** Writing – review & editing, Writing – original draft, Resources. **Oliver Plettenburg:** Writing – review & editing, Writing – original draft, Resources, Methodology, Formal analysis. **Vasilis Ntziachristos:** Writing – review & editing, Writing – original draft, Supervision, Resources, Investigation, Funding acquisition, Formal analysis.

Declaration of competing interest

V.N. is a founder and equity owner of sThesis GmbH, iThera Medical GmbH, Spear UG, and I3 Inc. The remaining authors declare no competing interests.

Data availability

Data will be made available on request.

Acknowledgements

This project has received funding from the European Research Council (ERC) under the European Union's Horizon 2020 research and innovation programme under grant agreement no. 694968 (PREMSOT). The research leading to these results was supported by the Deutsche Forschungsgemeinschaft (DFG), Germany (Gottfried Wilhelm Leibniz Prize 2013, NT 3/10–1) as well as by the DFG as part of the CRC 1123 (Z1). P. O'Connor, O. Plettenburg and M. Sattler acknowledge support from the Helmholtz Association and the Bundesministerium für Bildung und Forschung (BMBF) (16GW0251K). We wish to thank Dr. Jieying Zhou (from Dr. Jian Cui's lab) for TEM measurements, Dr. Juan Antonio Aguilar-Pimentel (German Mouse Clinic/Institute of Experimental Genetics, Helmholtz Zentrum München) for providing the thermal camera, and Dr. Doris Bengel for assisting with animal experimental procedures. We also wish to thank Dr. Gabriella Leung, Dr. Serene Lee and Dr. Elisa Bonnin for helpful suggestions on the manuscript.

Appendix A. Supplementary data

Supplementary data to this article can be found online at https://doi.

org/10.1016/j.jconrel.2024.06.037.

References

[1] N. Liu, P. O'Connor, V. Gujrati, D. Gorpas, S. Glasl, A. Blutke, A. Walch, K. Kleigrewe, M. Sattler, O. Plettenburg, V. Ntziachristos, Facile synthesis of a croconaine-based nanoformulation for OptA imaging and photothermal therapy, Adv. Healthc. Mater. 10 (9) (2021) 2002115.

[2] Y. Liu, P. Bhattarai, Z. Dai, X. Chen, Photothermal therapy and photoacoustic imaging via nanotheranostics in fighting cancer, Chem. Soc. Rev. 48 (7) (2019) 2053–2108.

[3] N. Liu, V. Gujrati, J.P.F. Werner, K. Mishra, P. Anzenhofer, A.C. Stiel, G. Mettenleiter, A. Feuchtinger, A. Walch, V. Ntziachristos, Bacterial outer membrane vesicles as cationic dye carriers for OptAs-guided phototherapy of cancer, Cancer Nanotechnol. 14 (1) (2023) 36.

[4] X. Chen, X. Ma, G. Yang, G. Huang, H. Dai, N. Liu, J. Yu, Squaraine nanoparticles for OptA imaging-guided synergistic cancer phototherapy, Nanophotonics 12 (18) (2023) 3645–3652.

[5] D. Zhi, T. Yang, J. O'Hagan, S. Zhang, R.F. Donnelly, Photothermal therapy, J. Control. Release 49 (3) (2022) 847–860.

[6] N. Liu, P. O'Connor, V. Gujrati, P. Anzenhofer, U. Klemm, K. Kleigrewe, M. Sattler, O. Plettenburg, V. Ntziachristos, Multifunctional croconaine nanoparticles for efficient OptA imaging of deep tumors and photothermal therapy, Nanophotonics 11 (21) (2022) 4637–4647.

[7] N. Liu, K. Mishra, A.C. Stiel, V. Gujrati, V. Ntziachristos, The sound of drug delivery: OptA imaging in pharmacology, Adv. Drug Deliv. Rev. 189 (2022) 114506.

[8] D. Razansky, J. Klohs, R. Ni, Multi-scale OptA molecular imaging of brain diseases, Eur. J. Nucl. Med. Mol. Imaging 48 (13) (2021) 4152–4170.

[9] C. Yin, X. Li, Y. Wang, Y. Liang, S. Zhou, P. Zhao, C.S. Lee, Q. Fan, W. Huang, Organic semiconducting macromolecular dyes for NIR-II photoacoustic imaging and Photothermal therapy, Adv. Funct. Mater. 31 (37) (2021) 2104650.

[10] N. Liu, X. Chen, M.A. Kimm, M. Stechele, X. Chen, Z. Zhang, M. Wildgruber, X. Ma, In vivo optical molecular imaging of inflammation and immunity, J. Mol. Med. 99 (10) (2021) 1385–1398.

[11] Z. Jiang, C. Zhang, X. Wang, M. Yan, Z. Ling, Y. Chen, Z. Liu, A borondifluoride-complex-based photothermal agent with an 80% photothermal conversion efficiency for photothermal therapy in the NIR-II window, Angew. Chem. Int. Ed. 60 (41) (2021) 22376–22384.

[12] S. Guo, D. Gu, Y. Yang, J. Tian, X. Chen, Near-infrared photodynamic and photothermal co-therapy based on organic small molecular dyes, J. Nanobiotechnol. 21 (1) (2023) 348.

[13] C. Jeong, S. Uthaman, B. Bagheri, J. Kim, S. Pillarisetti, I.-K. Park, Y.-C. Kim, Self-assembled heptamethine cyanine dye dimer as a novel theranostic drug delivery carrier for effective image-guided chemo-photothermal cancer therapy, J. Control. Release 329 (2021) 50–62.

[14] J. Mu, M. Xiao, Y. Shi, X. Geng, H. Li, Y. Yin, X. Chen, The chemistry of organic contrast agents in the NIR-II window, Angew. Chem. Int. Ed. 61 (14) (2022) e202114722.

[15] H.A. Shindy, Fundamentals in the chemistry of cyanine dyes: a review, Dyes Pigments 145 (2017) 505–513.

[16] S. Zhu, R. Tian, A.L. Antaris, X. Chen, H. Dai, Near-infrared-II molecular dyes for cancer imaging and surgery, Adv. Mater. 31 (24) (2019) e1900321.

[17] C. Shi, J.B. Wu, D. Pan, Review on near-infrared heptamethine cyanine dyes as theranostic agents for tumor imaging, targeting, and photodynamic therapy, J. Biomed. Opt. 21 (5) (2016) 050901.

[18] J.A. Carr, D. Franke, J.R. Caram, C.F. Perkinson, M. Saif, V. Askoxylakis, M. Datta, D. Fukumura, R.K. Jain, M.G. Bawendi, O.T. Bruns, Shortwave infrared fluorescence imaging with the clinically approved near-infrared dye indocyanine green, Proc. Natl. Acad. Sci. 115 (17) (2018) 4465–4470.

[19] K. Bilici, S. Cetin, E. Aydindogan, H. Yagci Acar, S. Kolemen, Recent advances in cyanine-based phototherapy agents, Front. Chem. 9 (2021) 707876.

[20] R.E. Borg, J. Rochford, Molecular photoacoustic contrast agents: design principles & applications, Photochem. Photobiol. 94 (6) (2018) 1175–1209.

[21] S. Onoe, T. Temma, K. Kanazaki, M. Ono, H. Saji, Development of photostabilized asymmetrical cyanine dyes for in vivo photoacoustic imaging of tumors, J. Biomed. Opt. 20 (9) (2015) 096006.

[22] E. Feng, L. Jiao, S. Tang, M. Chen, S. Lv, D. Liu, J. Song, D. Zheng, X. Peng, F. Song, Anti-photobleaching cyanine-based nanoparticles with simultaneous PET and ACQ effects for improved tumor photothermal therapy, Chem. Eng. J. 432 (2022) 134355.

[23] X. Mu, Y. Lu, F. Wu, Y. Wei, H. Ma, Y. Zhao, J. Sun, S. Liu, X. Zhou, Z. Li, Supramolecular nanodiscs self-assembled from non-ionic heptamethine cyanine for imaging-guided cancer photothermal therapy, Adv. Mater. 32 (2) (2019) e1906711.

[24] G. Fei, S. Ma, C. Wang, T. Chen, Y. Li, Y. Liu, B. Tang, T.D. James, G. Chen, Imaging strategies using cyanine probes and materials for biomedical visualization of live animals, Coord. Chem. Rev. 447 (2021) 214134.

[25] X. Meng, J. Zhang, Z. Sun, L. Zhou, G. Deng, S. Li, W. Li, P. Gong, L.J.T. Cai, Hypoxia-triggered single molecule probe for high-contrast NIR II/PA tumor imaging and robust photothermal therapy, Theranostics 8 (21) (2018) 6025.

[26] R.M. Exner, F. Cortezon-Tamarit, S.I. Pascu, Explorations into the effect of meso-substituents in tricarbocyanine dyes: a path to diverse biomolecular probes and materials, Angew. Chem. Int. Ed. 60 (12) (2021) 6230–6241.

[27] G. Yin, Y. Ma, Y. Xiong, X. Cao, Y. Li, L. Chen, Enhanced AIE and different stimuli-responses in red fluorescent (1,3-dimethyl)barbituric acid-functionalized anthracenes, J. Mater. Chem. C 4 (4) (2016) 751–757.

[28] G.W.P. van Pruissen, J. Brebels, K.H. Hendriks, M.M. Wienk, R.A.J. Janssen, Effects of cross-conjugation on the optical absorption and frontier orbital levels of donor–acceptor polymers, Macromolecules 48 (8) (2015) 2435–2443.

[29] T. Karatsu, M. Yanai, S. Yagai, J. Mizukami, T. Urano, A. Kitamura, Evaluation of sensitizing ability of barbiturate-functionalized non-ionic cyanine dyes; application for photoinduced radical generation system initiated by near IR light, J. Photochem. Photobiol. A Chem. 170 (2) (2005) 123–129.

[30] F. Lazreg, J. Loccufier, Near infrared (NIR) laser markable compositions, U.S. Patent Application No. 16/627,428, 2020.

[31] Q.-Q. Shi, R. Sun, J.-F. Ge, Q.-F. Xu, N.-J. Li, J.-M. Lu, A comparative study of symmetrical and unsymmetrical trimethine cyanine dyes bearing benzoxazolyl and benzothiazolyl groups, Dyes Pigments 93 (1) (2012) 1506–1511.

[32] H. Itokawa, S. Kameyama, T. Inaba, T. Tazaki, R. Haruta, Y. Kawazoe, M. Maeda, Radical methylation and radical hydroxymethylation of n-substituted quinoline derivatives, Chem. Pharm. Bull. 26 (4) (1978) 1015–1020.

[33] T. Yang, L. Liu, Y. Deng, Z. Guo, G. Zhang, Z. Ge, H. Ke, H. Chen, Ultrastable near-infrared conjugated-polymer nanoparticles for dually photoactive tumor inhibition, Adv. Mater. 29 (31) (2017) 1700487.

[34] M. Casalboni, F. De Matteis, P. Prosposito, A. Quatela, F. Sarcinelli, Fluorescence efficiency of four infrared polymethine dyes, Chem. Phys. Lett. 373 (3–4) (2003) 372–378.

[35] J.P. Fuenzalida Werner, Y. Huang, K. Mishra, R. Janowski, P. Vetschera, C. Heichler, A. Chmyrov, C. Neufert, D. Niessing, V. Ntziachristos, A.C. Stiel, Challenging a preconception: OptA spectrum differs from the optical absorption spectrum of proteins and dyes for molecular imaging, Anal. Chem. 92 (15) (2020) 10717–10724.

[36] Z. Chen, X.L. Dean-Ben, S. Gottschalk, D. Razansky, Performance of OptA and fluorescence imaging in detecting deep-seated fluorescent agents, Biomed. Opt. Express 9 (5) (2018) 2229–2239.

[37] D.K. Roper, W. Ahn, M. Hoepfner, Microscale heat transfer transduced by surface plasmon resonant gold nanoparticles, J. Phys. Chem. C 111 (9) (2007) 3636–3641.

[38] N. Liu, V. Gujrati, J. Malekzadeh-Najafabadi, J.P.F. Werner, U. Klemm, L. Tang, Z. Chen, J. Prakash, Y. Huang, A. Stiel, G. Mettenleiter, M. Aichler, A. Blutke, A. Walch, K. Kleigrewe, D. Razansky, M. Sattler, V. Ntziachristos, Croconaine-based nanoparticles enable efficient OptA imaging of murine brain tumors, Photoacoustics 22 (2021) 100263.

[39] Y. Pang, S. Fan, Q. Wang, D. Oprych, A. Feilen, K. Reiner, D. Keil, Y.L. Slominsky, S. Popov, Y. Zou, B. Strehmel, NIR-sensitized activated photoreaction between cyanines and oxime esters: free-radical photopolymerization, Angew. Chem. Int. Ed. 59 (28) (2020) 11440–11447.

[40] C. Kütahya, C. Schmitz, V. Strehmel, Y. Yagci, B. Strehmel, Near-infrared sensitized photoinduced atom-transfer radical polymerization (ATRP) with a copper(II) catalyst concentration in the ppm range, Angew. Chem. Int. Ed. 57 (26) (2018) 7898–7902.

[41] M.J. Frisch, G.W. Trucks, H.B. Schlegel, G.E. Scuseria, M.A. Robb, J.R. Cheeseman, G. Scalmani, V. Barone, G.A. Petersson, H. Nakatsuji, X. Li, M. Caricato, A. V. Marenich, J. Bloino, B.G. Janesko, R. Gomperts, B. Mennucci, H.P. Hratchian, J. V. Ortiz, A.F. Izmaylov, J.L. Sonnenberg, D. Williams-Young, F. Ding, F. Lipparini, F. Egidi, J. Goings, B. Peng, A. Petrone, T. Henderson, D. Ranasinghe, V. G. Zakrzewski, J. Gao, N. Rega, G. Zheng, W. Liang, M. Hada, M. Ehara, K. Toyota, R. Fukuda, J. Hasegawa, M. Ishida, T. Nakajima, Y. Honda, O. Kitao, H. Nakai, T. Vreven, K. Throssell, J.A. Montgomery Jr., J.E. Peralta, F. Ogliaro, M. J. Bearpark, J.J. Heyd, E.N. Brothers, K.N. Kudin, V.N. Staroverov, T.A. Keith, R. Kobayashi, J. Normand, K. Raghavachari, A.P. Rendell, J.C. Burant, S.S. Iyengar, J. Tomasi, M. Cossi, J.M. Millam, M. Klene, C. Adamo, R. Cammi, J.W. Ochterski, R.L. Martin, K. Morokuma, O. Farkas, J.B. Foresman, D.J. Fox, Gaussian 16 Revision C.01, Gaussian, Inc., Wallingford CT, 2016.

[42] M. Lepore, I. Delfino, Intralipid-based phantoms for the development of new optical diagnostic techniques, Open Biotechnol. J. 13 (1) (2019) 163–172.

[43] A. Rehman, I. Ahmad, K. Rehman, S. Anwar, S. Firdous, M. Nawaz, Optical properties measurement of highly diffusive tissue phantoms for biomedical applications, Laser Phys. 25 (2) (2015) 025605.

[44] V. Gujrati, J. Prakash, J. Malekzadeh-Najafabadi, A. Stiel, U. Klemm, G. Mettenleiter, M. Aichler, A. Walch, V. Ntziachristos, Bioengineered bacterial vesicles as biological nano-heaters for OptA imaging, Nat. Commun. 10 (1) (2019) 1114.

[45] X. Chen, X. Ma, G. Yang, G. Huang, H. Dai, J. Yu, N. Liu, Chalcogen atom-modulated croconaine for efficient NIR-II photothermal theranostics, ACS Appl. Mater. Interfaces 16 (10) (2024) 12332–12338.

[46] J. Li, X. Su, N. Liu, Synchronously manipulating absorption and nonradiative transition of croconaine via donor engineering for efficient NIR-II photothermal theranostics, Sensors Actuators B Chem. 408 (2024) 135535.

[47] Y.F. Xiao, C. Xiang, S. Li, C. Mao, H. Chen, J.X. Chen, S. Tian, X. Cui, Y. Wan, Z. Huang, X. Li, X.H. Zhang, W. Guo, C.S. Lee, Single-photomolecular nanotheranostics for synergetic near-infrared fluorescence and photoacoustic imaging-guided highly effective photothermal ablation, Small 16 (2020) e2002672.